

# DESIGN OF X-BAND BICONTROLLABLE METASURFACE ABSORBER COMPRISING GRAPHENE PIXELS ON COPPER-BACKED YIG SUBSTRATE

Govindam Sharma<sup>1</sup>, Akhlesh Lakhtakia<sup>2</sup>, and Pradip Kumar Jain<sup>1</sup>

<sup>1</sup>Department of Electronics and Communication Engineering, National Institute Technology Patna, Patna 800005, India

<sup>2</sup>Department of Engineering Science and Mechanics, The Pennsylvania State University, University Park, PA 16802, USA

## Abstract

The planewave response of a bicontrollable metasurface absorber with graphene-patched pixels was simulated in the X band using commercial software. Each square meta-atom is a  $4 \times 4$  array of 16 pixels, some patched with graphene and the others unpatched. The pixels are arranged on a PVC skin which is placed on a copper-backed YIG substrate. Graphene provides electrostatic controllability and YIG provides magnetostatic controllability. Our design delivers absorptance  $\geq 0.9$  over a 100-MHz spectral regime in the X band, with  $360 \text{ MHz kA}^{-1} \text{ m}$  magnetostatic controllability rate and  $1 \text{ MHz V}^{-1} \mu\text{m}$  electrostatic controllability rate. Notably, electrostatic control *via* graphene in the GHz range is novel.

**Keywords:** Bicontrollability, Magnetostatic controllability, Electrostatic controllability, Pixelation, Graphene, Yttrium iron garnet, Meta-atom, Metasurface, GHz.

## 1 Introduction

Metasurfaces are thin compared to the operational wavelength, accounting for their popularity in the R&D arena. The use of materials that respond electromagnetically to a stimulus allows controllable metasurfaces to be designed for beam-steering reflectors/filters [1], mirrors/lenses with variable focus [2], and absorbers/filters [3, 4] in a wide spectrum beginning with the microwave frequencies and ending with the visible frequencies.

Typically, controllable metasurfaces are designed to operate at high frequencies [5]. Direct scaling [6, 7] of controllable metasurface absorbers from THz frequencies to GHz frequencies is not always feasible, since constitutive parameters are frequency dependent. Generally, at GHz frequencies, metal is used to design the top layer of the metasurface, but using materials such as ferrites [8], graphene [9], and conductive rubber [10] allow control of metasurface absorbers.

Huang *et al.* experimentally demonstrated a magnetostatically controllable (or tunable) X-band absorber containing a ferrite slab, with a 300-MHz controllability range for absorptance  $A > 0.9$  [8]. Fallahi *et al.* design an electrostatically controllable metasurface absorber containing patterned graphene—but only the maximum absorptance  $A_{\text{max}}$ , not the maximum-absorptance frequency  $f_{\text{max}A}$ , can be controlled with that design [11]. Yi *et al.* used shape memory polymers to thermally control  $f_{\text{max}A} \in [11.3, 13.5] \text{ GHz}$  [12]. None of these metasurface absorbers covers the complete X band with absorptance in excess of 0.9, which is an important requirement for wide use.

Bicontrollable X-band metasurface absorbers are desirable for weather radar, police speed radar, and direct broadcast television. With that in mind, Sharma *et al.* designed a pixellated metasurface absorber with coarse magnetostatic and fine thermal controllability of  $f_{\max A}$  over the entire X band

[13]. The meta-atoms in this design comprise yttrium iron garnet (YIG)-patched pixels and conductive rubber (CR)-patched pixels on a metal-backed silicon substrate.

Continuing in the same vein, we are now reporting a pixelated metasurface absorber with  $f_{\max A}$  controllable both magnetostatically and electrostatically in the entire X band, while keeping  $A \geq 0.9$  over a 100-MHz spectral regime. Each meta-atom is a  $N_r \times N_r$  array of pixels, some patched with graphene and the others unpatched. In contrast to numerous designs [14, 15], the patches are not metallic. The pixels are arranged on a PVC skin which is placed on top of a copper-backed YIG substrate. Graphene provides electrostatic controllability and YIG provides magnetostatic controllability. Pixel size as well as the configuration of patched pixels were decided by examining the absorbance spectrums of many designs.

The plan of this paper is as follows. Section 2 provides information on the metasurface geometry, the relative permeability dyadic of YIG, the surface conductivity of graphene, and theoretical simulations. Numerical results are presented and discussed in Sec. 3. Some remarks in Sec. 4 conclude the paper.

An  $\exp(j\omega t)$  dependence on time  $t$  is implicit, with  $j = \sqrt{-1}$ ,  $\omega = 2\pi f$  as the angular frequency, and  $f$  as the linear frequency. The free-space wavenumber is denoted by  $k_0 = \omega \sqrt{\varepsilon_0 \mu_0} = 2\pi/\lambda_0$ , where  $\lambda_0$  is the free-space wavelength,  $\varepsilon_0$  is the free-space permittivity, and  $\mu_0$  is the free-space permeability. Vectors are denoted by boldface letters; the Cartesian unit vectors are denoted by  $\hat{\mathbf{x}}$ ,  $\hat{\mathbf{y}}$ , and  $\hat{\mathbf{z}}$ ; and dyadics are double underlined.

## 2 Materials and Methods

### 2.1 Device Structure

The metasurface extends to infinity in all directions in the  $xy$  plane, but it is of finite thickness along the  $z$  axis, as depicted in Fig. 1. The metasurface is a biperiodic array of square meta-atoms whose sides are aligned along the  $x$  and  $y$  axes.

Each meta-atom is of side  $a$ . The front surface of the meta-atom is an array of  $N_r \times N_r$  square pixels of side  $b$ , each pixel separated from every neighboring pixel by a distance  $d \ll a$ , so that  $N_r = a/(b + d)$ . Some of the pixels are patched with graphene, but others are not. Underneath the pixels is a polyvinyl-chloride (PVC) skin of thickness  $L_{\text{PVC}}$ , a YIG substrate of thickness  $L_{\text{sub}}$ , and a copper sheet of thickness  $L_{\text{m}}$  serving as a back reflector.

We fixed  $N_r = 4$ ,  $L_{\text{PVC}} = 0.08$  mm,  $L_{\text{sub}} = 0.2$  mm, and  $L_{\text{m}} = 0.07$  mm. In addition, we fixed  $a = 6$  mm,  $b = 1.45$  mm, and  $d = 0.05$  mm, after multiple iterations of parameter sweeps.

### 2.2 YIG

The relative permeability dyadic  $\underline{\underline{\mu}}_{\text{YIG}}$  of YIG depends on the magnitude and direction of the external magnetostatic field  $\mathbf{H}_0$ . With this field aligned along the  $x$  axis (i.e,  $\mathbf{H}_0 = H_0 \hat{\mathbf{x}}$ ), we have [16]

$$\underline{\underline{\mu}}_{\text{YIG}} = \hat{\mathbf{x}}\hat{\mathbf{x}} + \mu_{\text{yy}} (\hat{\mathbf{y}}\hat{\mathbf{y}} + \hat{\mathbf{z}}\hat{\mathbf{z}}) + j\mu_{\text{yz}} (\hat{\mathbf{y}}\hat{\mathbf{z}} - \hat{\mathbf{z}}\hat{\mathbf{y}}), \quad (1a)$$

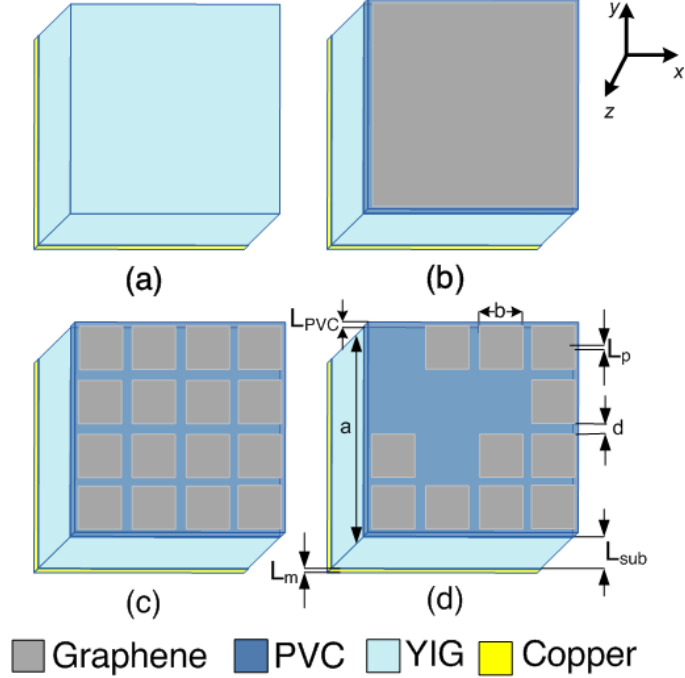


Figure 1: Schematics of four meta-atoms: (a) copper-backed YIG substrate; (b) graphene on top of a PVC skin overlaying a copper-backed YIG substrate; (c) the same as (b) but with graphene partitioned as a  $4 \times 4$  array of graphene patches; and (d) the same as (c) but with only ten pixels patched with graphene. The Cartesian coordinate system is also shown.

where

$$\mu_{yy} = 1 + \frac{4\pi\mu_0^2\gamma M_s \left(H_0 + j\frac{\Delta H}{2}\right)}{(\mu_0\gamma)^2 \left(H_0 + j\frac{\Delta H}{2}\right)^2 - \omega^2} \quad (1b)$$

and

$$\mu_{yz} = \frac{4\pi\omega\mu_0\gamma M_s}{(\mu_0\gamma)^2 \left(H_0 + j\frac{\Delta H}{2}\right)^2 - \omega^2}. \quad (1c)$$

In these equations,  $\gamma = 1.76 \times 10^{11} \text{ C kg}^{-1}$  is the gyromagnetic ratio,  $\Delta H = 1.98 \text{ kA m}^{-1}$  is the resonance linewidth, and  $M_s = 0.18 \text{ Wb m}^{-2}$  is the saturation magnetization. The relative permittivity scalar of YIG is  $\epsilon_{\text{YIG}} = 15$ . Note that  $H_0\hat{x}$  can be applied by placing the metasurface between two magnets, so long as the lateral extent of the metasurface is in excess of  $10\lambda_0$ .

### 2.3 Graphene

Graphene is not affected significantly by  $H_0\hat{x}$ , because that magnetostatic field is wholly aligned in the plane containing the carbon atoms [17]. It is, however, affected by the external electrostatic field  $\mathbf{E}_0 = E_0\hat{z}$  aligned normal to that plane, which can be applied using transparent electrodes significantly above and below the metasurface.

The surface conductivity of graphene  $\sigma_{\text{gr}}$  comprises an intraband term and an interband term, the latter being negligibly small compared to the former in the X band [17,18]. Accordingly,

$$\sigma_{\text{gr}} = -j \frac{q_e^2 k_B T}{\pi \hbar^2 (\omega - 2j\tau_{\text{gr}}^{-1})} \times \left\{ \frac{\mu_c}{k_B T} + 2 \ln \left[ 1 + \exp \left( -\frac{\mu_c}{k_B T} \right) \right] \right\}, \quad (2)$$

where  $q_e = 1.602\,177 \times 10^{-19}$  C is the elementary charge,  $k_B = 1.380\,649 \times 10^{-23}$  J K<sup>-1</sup> is the Boltzmann constant, and  $\hbar = 1.054\,572 \times 10^{-34}$  J s is the reduced Planck constant. All calculations were made for temperature  $T = 300$  K. We fixed the momentum relaxation time  $\tau_{\text{gr}} = 0.4$  ps after examining values of the maximum absorptance  $A_{\text{max}}$  and the controllability rate  $\partial f_{\text{maxA}}/\partial E_0$  for  $\tau_{\text{gr}} \in [0.01, 1]$  ps. This relaxation time can be controlled by impurity level [3].

The value of the chemical potential  $\mu_c$  depends on  $E_0$  as well as on the d.c. relative permittivity  $\varepsilon_{\text{PVC}} = 2.7$  of PVC [19]. Thus [4,17],

$$\frac{\pi \varepsilon_0 \hbar^2 v_F^2}{q_e k_B^2 T^2} \varepsilon_{\text{PVC}} E_0 = \text{Li}_2 \left[ -\exp \left( -\frac{\mu_c}{k_B T} \right) \right] - \text{Li}_2 \left[ -\exp \left( \frac{\mu_c}{k_B T} \right) \right], \quad (3)$$

where  $v_F = 10^6$  m s<sup>-1</sup> [20] is the Fermi speed for graphene and  $\text{Li}_\nu(\zeta)$  is the polylogarithm function of order  $\nu$  and argument  $\zeta$  [21]. The Newton–Raphson technique [22] was used to determine  $\mu_c$  as a function of  $E_0$ .

## 2.4 Theoretical Simulations

The pixels of the metasurface were taken to be illuminated by a normally incident, linearly polarized plane wave whose electric field phasor can be written as

$$\mathbf{E}^{\text{inc}} = \alpha \hat{\mathbf{x}} \exp(-jk_0 z), \quad (4)$$

with  $\alpha$  as its amplitude.

As the metasurface is periodic along the  $x$  and  $y$  axes, the reflected field must be written as a doubly infinite series of Floquet harmonics [23]. Since  $a < \lambda_0/4$  in the entire X band, only specular components of the reflected field are non-evanescent. Therefore, the reflected electric field as  $z \rightarrow -\infty$  may be written as

$$\mathbf{E}^{\text{ref}} \simeq \alpha (\rho_{\text{xx}} \hat{\mathbf{x}} + \rho_{\text{yx}} \hat{\mathbf{y}}) \exp(jk_0 z), \quad (5)$$

where  $\rho_{\text{xx}} \in \mathbb{C}$  is the co-polarized reflection coefficient and  $\rho_{\text{yx}} \in \mathbb{C}$  is the cross-polarized reflection coefficient. The transmitted field in the region beyond the metallic back reflector was negligibly small in magnitude, because  $L_m$  is much larger than the penetration depth in copper. Hence, the absorptance was calculated as

$$A = 1 - (|\rho_{\text{xx}}|^2 + |\rho_{\text{yx}}|^2). \quad (6)$$

Normal incidence on several configurations of the pixelated-metasurface absorber was simulated using the commercial tool CST Microwave Studio<sup>TM</sup> 2020. Periodic boundary conditions were applied

along the  $x$  and  $y$  axes. The option OPEN was chosen for the  $z$  axis and the PLANEWAVE condition applied. The meta-atom was partitioned into as many as 10,026 tetrahedrons for each simulation in order to achieve convergent results. The absorptance  $A$  was calculated for  $f \in [8, 12]$  GHz,  $H_0 \in [180, 270]$  kA m<sup>-1</sup>, and  $E_0 \in [0, 100]$  V μm<sup>-1</sup>.

### 3 Numerical Results

We begin by discussing the response of the copper-backed YIG substrate shown in Fig. 1(a). Figure 2(a) shows the computed spectrums of  $A$  for  $H_0 \in \{180, 210, 240, 270\}$  kA m<sup>-1</sup>, this metasurface being unaffected by  $E_0$ . The maximum-absorptance frequency  $f_{\max A}$  blueshifts as the magneto-static field  $H_0$  increases, but the maximum absorptance  $A_{\max} \leq 0.8$ . Hence, the copper-backed YIG substrate does not satisfy the requirement of  $A_{\max} \in [0.9, 1]$  in any spectral regime within the X band.

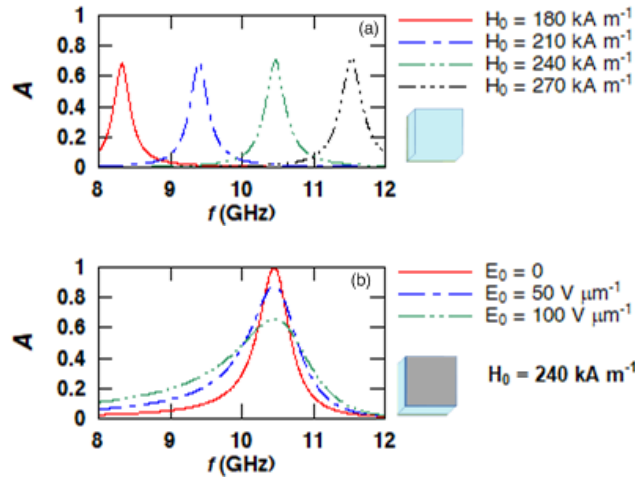


Figure 2: Absorptance spectrums of (a) the YIG/copper structure of Fig. 1(a) for  $H_0 \in \{180, 210, 240, 270\}$  kA m<sup>-1</sup> and (b) the graphene/PVC/YIG/copper structure of Fig. 1(b) for  $E_0 \in \{0, 50, 100\}$  V μm<sup>-1</sup> and  $H_0 = 240$  kA m<sup>-1</sup>.

Covering the YIG substrate on the top, first by a PVC skin and then by graphene, as in Fig. 1(b), certainly affects the absorptance. Graphene makes this structure susceptible to  $E_0$ , in addition to the YIG-mediated susceptibility to  $H_0$ . The spectrums of  $A$  are shown in Fig. 2(b) for  $E_0 \in \{0, 50, 100\}$  V μm<sup>-1</sup> and  $H_0 = 240$  kA m<sup>-1</sup>. Now,  $A_{\max}$  becomes a decreasing function of  $E_0$ , although the controllability of  $f_{\max A}$  by  $H_0$  (results not shown) is maintained. Therefore, the copper-backed YIG substrate with or without the graphene/PVC bilayer is inadequate as the desired bicontrollable metasurface absorber.

For the next set of simulations, we partitioned the graphene in Fig. 1(b) into 16 patches per meta-atom, as shown in Fig. 1(c). The absorptance spectrums in Fig. 3(a) for  $E_0 \in \{0, 50, 100\}$  V μm<sup>-1</sup> and  $H_0 = 240$  kA m<sup>-1</sup> clearly indicate that pixelation can increase  $A_{\max}$  and make it less susceptible to variations in  $E_0$ , when compared with the spectrums in Fig. 2(b). The

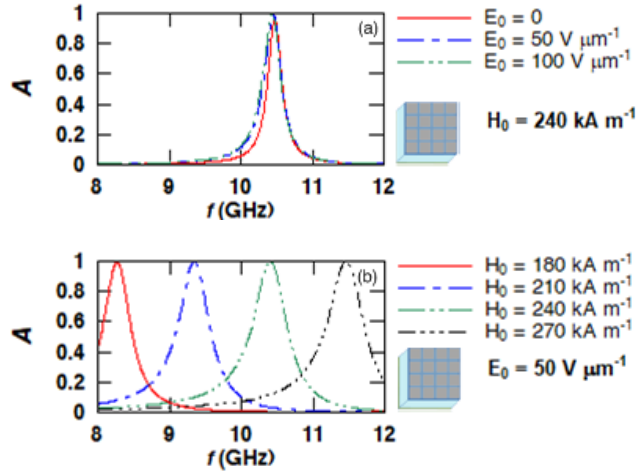


Figure 3: Absorptance spectrums of the pixelated metasurface of Fig. 1(c), with all 16 pixels per meta-atom patched with graphene. (a)  $E_0 \in \{0, 50, 100\} \text{ V } \mu\text{m}^{-1}$  and  $H_0 = 240 \text{ kA m}^{-1}$ . (b)  $H_0 \in \{180, 210, 240, 270\} \text{ kA m}^{-1}$  and  $E_0 = 50 \text{ V } \mu\text{m}^{-1}$ .

absorptance spectrums in Fig. 3(b) for  $H_0 \in \{180, 210, 240, 270\} \text{ kA m}^{-1}$  and  $E_0 = 50 \text{ V } \mu\text{m}^{-1}$  confirm the magnetostatic controllability of  $f_{\max A}$ .

Finally, we present the absorptance spectrums calculated for the metasurface of Fig. 1(d), which has ten graphene-patched and six unpatched pixels. The specific configuration of unpatched pixels was selected after studying the absorption spectrums for many other configurations. The spectrums in Fig. 4(a) for  $E_0 \in \{0, 50, 100\} \text{ V } \mu\text{m}^{-1}$  and  $H_0 = 240 \text{ kA m}^{-1}$  and Fig. 4(b) for  $H_0 \in \{180, 210, 240, 270\} \text{ kA m}^{-1}$  and  $E_0 = 50 \text{ V } \mu\text{m}^{-1}$  indicate that a bicontrollable spectral regime with  $A \geq 0.9$  and  $A_{\max} \approx 0.99$  can be achieved with  $360 \text{ MHz kA}^{-1} \text{ m}$  magnetostatic control and  $1 \text{ MHz V}^{-1} \mu\text{m}$  electrostatic control of  $f_{\max A}$ . Coarse control is possible through  $H_0$  and fine control through  $E_0$ . The bandwidth  $\Delta f_{A \geq 0.9}$  of this absorber is about 100 MHz, which is suitable for many X-band applications.

Table 1 compares the proposed metasurface absorber with previously reported absorbers. Yuan *et al.* [24] designed a voltage-controlled metasurface absorber containing varactor diodes, for X-band operation with  $f_{\max A}$  controlled in a 440-MHz range. Huang *et al.* [8] incorporated a meta-atom with a metal resonator printed on FR4 and affixed to a metal-backed ferrite substrate. Their metasurface absorber has a wider bandwidth than the proposed absorber redhas, but the controllability range is smaller than of the proposed absorber. Sharma *et al.* [13] reported a meta-atom with a square array of pixels patched with conductive rubber and YIG on a metal-backed silicon substrate. This bicontrollable metasurface has a wider bandwidth with stable maximum absorptance in the entire X band, and fine control is thermal rather than electrostatic as for the proposed absorber.

I

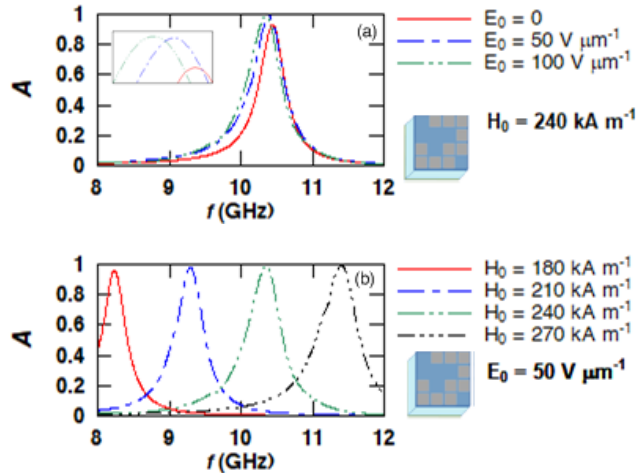


Figure 4: Absorptance spectrums of the pixelated metasurface of Fig. 1(d), with only 10 pixels per meta-atom patched with graphene. (a)  $E_0 \in \{0, 50, 100\} \text{ V } \mu\text{m}^{-1}$  and  $H_0 = 240 \text{ kA m}^{-1}$ . (b)  $H_0 \in \{180, 210, 240, 270\} \text{ kA m}^{-1}$  and  $E_0 = 50 \text{ V } \mu\text{m}^{-1}$ .

## 4 Concluding Remarks

We conceived, designed, and investigated a electrostatically and magnetostatically controllable metasurface absorber for operation in the entire X band. The meta-atom comprises ten graphene-patched pixels and six unpatched pixels in a  $4 \times 4$  array on a PVC skin that is affixed to a metal-backed YIG substrate. Graphene provides electrostatic controllability and YIG provides magnetostatic controllability. Electrostatic control of the maximum-absorptance frequency using graphene-patched pixels in the GHz range is novel. The configuration of graphene-patched and unpatched pixels was optimized to achieve stable maximum absorptance of 0.99, with pixelation performing better than continuous graphene. According to our simulations, the chosen design delivers absorptance  $\geq 0.9$  over a 100-MHz band, with  $360 \text{ MHz kA}^{-1} \text{ m}$  magnetostatic controllability rate and  $1 \text{ MHz V}^{-1} \mu\text{m}$  electrostatic controllability rate. The proposed X-band absorber can be used to improve the performance of radar systems.

## References

- [1] Wu PC, Pala RA, Shirmanesh GK, Cheng W-H, Sokhoyan R, Grajower M, Alam MZ, Lee D, Atwater HA. Dynamic beam steering with all-dielectric electro-optic III–V multiple-quantum-well metasurfaces. *Nat. Commun.* 2019;10(1):3654.
- [2] Ding P, Li Y, Shao L, Tian X, Wang J, Fan C. Graphene aperture-based metalens for dynamic focusing of terahertz waves. *Opt. Exp.* 2018;26(21):28038–28050.
- [3] Kumar P, Lakhtakia A, Jain PK. Tricontrollable pixelated metasurface for stopband for terahertz radiation. *J. Electromag. Waves Appl.* 2020;34(15):2065–2078.

Table 1: Structure, type of control, controllability range of maximum-absorptance frequency ( $f_{\max A}$ ), bandwidth ( $\Delta f_{A \geq 0.9}$ ), and controllability rate of reported metasurface absorbers and the proposed metasurface absorber.

Ref.	Structure	Control method(s)	$f_{\max A}$ (GHz)	$\Delta f_{A \geq 0.9}$ (MHz)	Controllability rate
8	Metal resonator/FR4/ferrite/metal sheet	magnetostatic	9.3–9.7	150	3 MHz $\text{kA}^{-1}$ m
24	Metal pads separated by varactor diodes/FR4 sheet/metal sheet	electrical	8.25–9.25	400	100 MHz $\text{V}^{-1}$
13	YIG- and CR-patched pixels/silicon/metal sheet	magnetostatic and thermal	8–13	200	360 MHz $\text{kA}^{-1}$ m and 1 MHz $\text{K}^{-1}$
This work	Graphene pixels/PVC skin/YIG/metal sheet	magnetostatic and electrostatic	8–12	100	360 MHz $\text{kA}^{-1}$ m and 1 MHz $\text{V}^{-1}$ $\mu\text{m}$

- [4] Kumar P, Lakhtakia A, Jain PK. Tricontrollable pixelated metasurface for absorbing terahertz radiation. *Appl. Opt.* 2019;58(35):9614–9623.
- [5] He Q, Sun S, Zhou L. Tunable/reconfigurable metasurfaces: physics and applications. *Research.* 2019;2019:1849272.
- [6] Sinclair G. Theory of models of electromagnetic systems. *Proc. IRE.* 1948;36(11):1364–1370.
- [7] Lakhtakia A. Scaling of fields, sources, and constitutive properties in bianisotropic media. *Microw. Opt. Technol. Lett.* 1994;7(7):328–330.
- [8] Huang Y, Wen G, Zhu W, Li J, Si LM, Premaratne M. Experimental demonstration of a magnetically tunable ferrite based metamaterial absorber. *Opt. Exp.* 2014;22(13):16408–16417.
- [9] Yi D, Wei XC, Xu YL. Tunable microwave absorber based on patterned graphene. *IEEE Trans. Microw. Theory Tech.* 2017;65(8):2819–2826.
- [10] Qiu K, Jin J, Liu Z, Zhang F, Zhang W. A novel thermo-tunable band-stop filter employing a conductive rubber split-ring resonator. *Mater. Des.* 2017;116:309–315.
- [11] Fallahi A, Perruisseau-Carrier J. Design of tunable biperiodic graphene metasurfaces. *Phys. Rev. B.* 2012; 86(19):195408.
- [12] Yi J, Wei M, Lin M, Zhao X, Zhu L, Chen X, Jiang ZH. Frequency-tunable and magnitude-tunable microwave metasurface absorbers enabled by shape memory polymers. *IEEE Trans. Antennas Propagat.* 2022;70(8):6804–6812.
- [13] Sharma G, Kumar P, Lakhtakia A, Jain PK. Pixelated bicontrollable metasurface absorber tunable in complete X band. *J. Electromag. Waves Appl.* 2022;36(17):2505-2518.

- [14] Mahabadi RK, Goudarzi T, Fleury R, Sohrabpour S, Naghdabadi R. Effects of resonator geometry and substrate stiffness on the tunability of a deformable microwave metasurface. *AEÜ Int. J. Electron. Commun.* 2022;146:154123.
- [15] Yousaf A, Murtaza M, Wakeel A, Anjum S. A highly efficient low-profile tetra-band metasurface absorber for X, Ku, and K band applications. *AEÜ Int. J. Electron. Commun.* 2022;154:154329.
- [16] Pozar DM. *Microwave engineering*. USA: Wiley;2011.
- [17] Hanson GW. Dyadic Green's functions for an anisotropic, non-local model of biased graphene. *IEEE Trans. Antennas Propagat.* 2008;56(3):747–757.
- [18] Geng M-Y, Liu Z-G, Wu W-J, Chen H, Wu B, Lu W-B. A dynamically tunable microwave absorber based on graphene. *IEEE Trans. Antennas Propagat.* 2020;68(6):4706–4713.
- [19] Riddle B, Baker-Jarvis J, Krupka J. Complex permittivity measurements of common plastics over variable temperatures. *IEEE Trans. Microw. Theory Tech.* 2003;51(3):727–733.
- [20] Novoselov KS, Geim AK, Morozov SV, Jiang D, Katsnelson MI, Grigorieva I, Dubonos S, Firsov A. Two-dimensional gas of massless Dirac fermions in graphene. *Nat.* 2005;438(7065):197–200.
- [21] Cvijović D. New integral representations of the polylogarithm function. *Proc. R. Soc. London A* 2007;463(2080):897–905.
- [22] Jaluria Y. *Computer methods for engineering*. Taylor & Francis;1996.
- [23] Ahmad F, Anderson TH, Civiletti BJ, Monk PB, Lakhtakia A. On optical-absorption peaks in a nonhomogeneous thin-film solar cell with a two-dimensional periodically corrugated metallic backreflector. *J. Nanophoton.* 2018;12(1):016017.
- [24] Yuan H, Zhu BO, Feng Y. A frequency and bandwidth tunable metamaterial absorber in X band. *J. Appl. Phys.* 2015;117(17):173103.